YIC2012 — Universidade de Aveiro
First ECCOMAS Young Investigators Conference
A. Andrade-Campos, N. Lopes, R.A.F. Valente, H. Varum (editors)
24–27 April 2012, Aveiro. Portugal.

Hybridizable Discontinuous Galerkin p-adaptivity for wave problems

G. Giorgiani [a,⋆], S. Fernandéz Mendéz [a], A. Huerta [a]

[a]Laboratori de Càlcul Numèric,
Departament de Matemàtica Aplicada III, E.T.S. de Ingenieros de Caminos
Universitat Politècnica de Catalunya – BarcelonaTech,
Jordi Girona 1, E-08034 Barcelona, Spain

⋆Corresponding author: giorgio.giorgiani@upc.edu

Abstract. *A p-adaptive Hybridizable Discontinuous Galerkin (HDG) method is presented for the solution of wave problems. The HDG method allows to drastically reduce the coupled degrees of freedom of the computation seeking for an approximation of the solution that is defined only on the edges of the mesh. The particular choice of the numerical fluxes driven by the hybridization technique allows to obtain an optimally converging solution not only for the primal unknown but also for its derivative. This characteristic allows to perform a post-process of the solution that provides a super-convergent solution.*
The discontinuous character of the solution provides an optimal framework for a p-adaptive technique. The post-processed solution of the HDG method is used to construct a cheap and reliable error estimator that drives an element by element modification of the approximation degree.
The proposed p-adaptive HDG method is compared with high-order CG computation with static condensation of the interior nodes. A challenging problem is considered for the comparison: a non-homogeneous scattering problem in an open domain.

Keywords: discontinuous Galerkin method; *p*-adaptivity; hybridization; high-order; HDG; wave propagation.

1 INTRODUCTION

Discontinuous Galerkin methods (DG) [1, 2], are finite element methods that are locally conservative and stable, and allow to achieve high order accuracy. The DG formulation uses discontinuous approximation element by element, with the information that passes through the elements by means of the numerical fluxes. Since their introduction, DG methods have been used to solve a great variety of partial differential equation, gaining an increasing interest in the scientific computing community since they have proved to be suited for the construction of robust high order numerical schemes on arbitrary unstructured and non-conforming grids for a variety of physical fenomena.
For second order elliptic problems DG methods are always hampered, compared to the continuous finite element method (CG), by their larger number of degrees of freedom (DOF). Nevertheless, recent contributions show more efficient DG computations compared with CG, for wave propagation problems. For instance in [3], the standard finite element basis is enriched with a set of planar waves defined in each element. Continuity between elements is imposed by means of Lagrange multipliers. This approach, despite very efficient, is restricted to constant wavelength in each element. In [4], the interior penalty discontinuous Galerkin performs better than CG in the pre-asymptotic range (large element size) for the Helmholtz equation. In [5], a discontinuous finite element formulation of the Helmholtz equation is proposed, which requires less DOF than the CG method for properly chosen parameters. In both [4] and [5], which are restricted to linear approximations and non-stabilized CG, the stabilization introduced by the numerical fluxes, and the subsequent reduction in dispersion error, clearly compensates the overhead in DOF of classic DG methods.
On the other hand, as shown next, high-order computations can be more efficient than low-order ones for wave problems. High-order elements, in this case $p > 2$, provide better accuracy for the same number of DOF, or require less computational cost for a desired accuracy level, even for engineering purpose. In the context of CG, the optimization technique known as static condensation allows to exploit the decoupling of local and global unknowns, reducing drastically the number of DOF of the problem. Until recently this type of optimization was not available

for DG methods. For this reason, classic DG methods, such as the Compact Discontinuous Galerkin method (CDG) [2], result inefficient compared to CG, for high order elements. However, the hybridizable discontinuous Galerkin method (HDG), see for example [6–8], is a novel DG method with unique characteristics: the hybridization technique allows to reduce the globally coupled DOF to those of an approximation of the solution defined solely on the sides of the mesh, recovering the elemental solution with a local computation. The similarity between hybridization in DG and static condensation in CG is highlighted in [9]. Similar performance of HDG and CG for the solution of the wave equation is shown here, for a wide range of wavelengths: HDG and CG provide similar accuracy for similar computational cost, when properly selecting *p* for a chosen error level and a given wavelength.
Obviously, adjusting locally the polynomial order of interpolation to the needs of a smooth solution, enables exploiting to the maximum the advantages of high-order elements. However, *p*-adaptive computations in the context of CG have had little success because they need special FE, such as FE with blending functions [10, 11], or mortar elements [12], to impose C_0 continuity of the approximation, leading to a cumbersome implementation. On the contrary, discontinuous Galerkin methods provide a natural framework for *p*-variable FE computations.
Furthermore, the particular flux choice in the HDG method provides an optimal converging approximation not only for the solution but also for its gradient. Then, an element-by-element post-process yields a superconvergent approximation. This characteristic, unique of the HDG method, is a major advantage for an adaptive technique: the post-process provides a reference solution that can be used for error estimation purpose. The error estimator induced by the HDG post-process proves to be reliable with very low computational cost.
The paper is organized as follows. Section 2 presents the *p*-variable HDG method for a non-constant coefficient Helmholtz-type wave equation, the Mild Slope Equation (MSE). Section 3 shows a comparison, with uniform *p*-distribution, between HDG, CG and CDG. Section 4 is devoted to the error estimation and the *p*-adaptive algorithm. A numerical example in Section 5 demonstrates the applicability and good performance of the proposed *p*-adaptive HDG method for problems of engineering interest such as wave propagation in harbors.

2 P-ADAPTIVE HDG FOR WAVE PROBLEMS

The MSE [13] is taken as model problem in an unbounded domain. The MSE describes the propagation of sea waves over a slow varying bathymetry, in shallow and deep water, for bottom slopes up to 1/3 [14]. The computational domain Ω is defined closing the unbounded domain with an artificial boundary, and a Perfectly Matched Layer (PML) [15] is used to minimize reflections from the artificial boundary. The problem statement is

$$\boldsymbol{\nabla\cdot}(cc_g\mathbf{P}\nabla\eta) + k^2 s_x s_y cc_g\eta = -s_x s_y(\boldsymbol{\nabla\cdot}(cc_g\nabla\eta_0) + k^2 cc_g\eta_0), \qquad \text{in } \Omega, \tag{1a}$$

$$\nabla\eta\cdot\boldsymbol{n} - ik\alpha\eta = -(\nabla\eta_0\cdot\boldsymbol{n} - ik\alpha\eta_0), \qquad \text{on } \Gamma_{\mathtt{R}}, \tag{1b}$$

$$\mathbf{P}\nabla\eta\cdot\boldsymbol{n} - ik\eta = 0, \qquad \text{on } \Gamma_{\mathtt{NRB}}. \tag{1c}$$

where $k(x,y)$ is the wave number, $\eta(x,y)$ denotes the reflected wave and $\eta_0 = \exp(ik_0\boldsymbol{d_0}\cdot\boldsymbol{x})$ is the incident wave, characterized by the wave number k_0 and its direction $\boldsymbol{d_0} = (\cos\theta_0, \sin\theta_0)$. The total wave is then $\hat{\eta} = \eta + \eta_0$. The parameters $c(x,y) \in \mathbb{R}$ and $c_g(x,y) \in \mathbb{R}$ are the wave celerity and the phase velocity. The Robin-type boundary conditions (1b) and (1c) are used to model respectively a partially absorbing boundary $\Gamma_{\mathtt{R}}$ (simulating for example dikes and breakwaters), with absorption coefficient α, and a first order absorbing artificial boundary $\Gamma_{\mathtt{NRB}}$. The vector $\boldsymbol{n}$ is the unitary outward normal at the boundary. Matrix $\mathbf{P}$ is the anisotropy matrix defining the absorption in the PML medium. Obviously, $\mathbf{P} = \mathbf{I}$ outside the PML. The absorption parameters in the two Cartesian directions are s_x and s_y. The wave number $k(x,y)$ is coupled with the bottom depth function $h(x,y)$ by means of the non-linear dispersion relation $\omega^2 = kg\tanh(kh)$, being g the gravity acceleration.
The domain Ω is partitioned in a set of $\mathtt{n_{el}}$ disjoint elements, $\mathcal{T}_h = \{K_j : j = 1, \ldots, \mathtt{n_{el}}\}$ with boundaries ∂K_j defining the set of element boundaries $\partial\mathcal{T}_h = \{\partial K : K \in \mathcal{T}_h\}$. For two neighboring elements K^+ and K^- of the collection $\mathcal{T}_h$, $\partial K^+ \cap \partial K^-$ is the interior side between K^+ and K^-, and for elements K along the boundary, $\partial K \cap \partial\Omega$ is the boundary side. The global set of interior and boundary sides is then denoted as $\mathcal{E}_h$. Edges are generically denoted by F, i.e. $F \in \mathcal{E}_h$.
The following finite element spaces $\boldsymbol{V}_h(\mathcal{T}_h)$, $P_h(\mathcal{T}_h)$ and $M_h(\mathcal{E}_h)$ associated to $\mathcal{T}_h$ and to $\mathcal{E}_h$ are also introduced

$$\begin{aligned}
\boldsymbol{V}_h &:= \left\{\boldsymbol{v} \in [L^2(\Omega)]^2 : \boldsymbol{v}|_K \in [\mathcal{P}^{p_K}(K)]^2, \forall K \in \mathcal{T}_h\right\},\\
P_h &:= \left\{q \in L^2(\Omega) : q|_K \in \mathcal{P}^{p_K}(K), \forall K \in \mathcal{T}_h\right\},\\
M_h &:= \left\{\mu \in L^2(\mathcal{E}_h) : \mu|_F \in \mathcal{P}^{p_F}(F), \forall F \in \mathcal{E}_h\right\},
\end{aligned}$$

where $\mathcal{P}^p$ denotes the space of polynomials of degree p, and p_K and p_F are the polynomial degrees in element K and side F respectively.

Remark 1 *In general, the polynomial degree for elements, and sides, can vary element by element, and side by side. More precisely, in all computations, given a map of elemental degrees, the interpolation degree p_F for a side shared by two elements, $F = \partial K^+ \cap \partial K^-$, is set as the maximum value of the degree in K^+ and K^-, that is $p_F = \max\{p_{K^+}, p_{K^-}\}$, and $p_F = p_K$ when $F \in \partial K \cap \partial\Omega$. This procedure ensures that for any element K the degree on all its sides is a least p_K, providing the desired accuracy in the element.*

The following scalar products are also defined

$$\big(\boldsymbol{v},\boldsymbol{\omega}\big)_K = \int_K \boldsymbol{v}\cdot\boldsymbol{\omega}\; d\Omega, \quad \big(p,q\big)_K = \int_K pq\; d\Omega, \quad \text{and} \quad \big\langle p,q\big\rangle_{\partial K} = \int_{\partial K} pq\; d\Gamma.$$

The HDG formulation is deduced from the first order system equivalent to (1a), namely

$$\begin{aligned}\boldsymbol{\nabla\cdot}\,\boldsymbol{\sigma} - \beta\eta &= f,\\ \mathbf{Q}^{-1}\boldsymbol{\sigma} + \boldsymbol{\nabla}\eta &= 0,\end{aligned}$$

with $f = s_x s_y(\boldsymbol{\nabla\cdot}\,(cc_g\nabla\eta_0) + k^2 cc_g\eta_0)$, $\beta = k^2 s_x s_y cc_g$ and $\mathbf{Q} = cc_g\mathbf{P}$. The discrete weak form is then stated for each element K: find $\boldsymbol{\sigma}_h \in \boldsymbol{V}_h$ and $\eta_h \in P_h$ such that

$$-\big(\boldsymbol{\sigma}_h,\boldsymbol{\nabla}q\big)_K - \big(\beta\eta_h,q\big)_K + \big\langle\hat{\boldsymbol{\sigma}}\cdot\boldsymbol{n},q\big\rangle_{\partial K} = \big(f,q\big)_K \qquad \forall q\in P_h, \tag{2}$$

$$\big(\mathbf{Q}^{-1}\boldsymbol{\sigma}_h,\boldsymbol{v}\big)_K - \big(\eta_h,\boldsymbol{\nabla\cdot}\,\boldsymbol{v}\big)_K + \big\langle\lambda,\boldsymbol{v}\cdot\boldsymbol{n}\big\rangle_{\partial K} = 0 \qquad \forall \boldsymbol{v}\in\boldsymbol{V}_h, \tag{3}$$

where $\hat{\boldsymbol{\sigma}}$ is a numerical flux and the subscript h is used to note that the unknowns of the problem have been replaced by their numerical counterpart. The trace variable $\lambda \in M_h$ along element sides is a new unknown introduced in (3) replacing the trace of η. The problem is closed adding a new equation imposing continuity of the normal component of the numerical flux $\hat{\boldsymbol{\sigma}}\cdot\boldsymbol{n}$ across the interior faces and the boundary conditions (1b) and (1c),

$$\big\langle\hat{\boldsymbol{\sigma}}\cdot\boldsymbol{n},\mu\big\rangle_{\partial\mathcal{T}_h} + i\big\langle cc_g k\alpha\lambda,\mu\big\rangle_{\Gamma_{\mathrm{R}}} + i\big\langle cc_g k\lambda,\mu\big\rangle_{\Gamma_{\mathrm{NRB}}} = \big\langle cc_g\left(\boldsymbol{\nabla}\eta_0\cdot\boldsymbol{n} - ik\alpha\eta_0\right),\mu\big\rangle_{\Gamma_{\mathrm{R}}}. \tag{4}$$

As specified in [7], the numerical flux is set in terms of λ as

$$\hat{\boldsymbol{\sigma}} = \boldsymbol{\sigma}_h + \tau(\eta_h - \lambda)\boldsymbol{n}, \tag{5}$$

where τ is a positive stabilization parameter. The influence of the τ parameter on the convergence properties of the HDG method has been studied in [7, 9]. In the present work, numerical experiments have led to the following choice for τ:

$$\tau = \begin{cases} 0, & \text{on } \partial K\backslash F^\tau,\\ 1000\frac{p_F^2}{kl_F}, & \text{on } F^\tau,\end{cases}$$

where F^τ is an arbitrary but fixed edge of K and l_F is the edge length.
Replacing (5) in (2) and in (4), and following [7], the HDG method for the MSE becomes: find $(\boldsymbol{\sigma}_h,\eta_h,\lambda) \in \boldsymbol{V}_h\times P_h\times M_h$ such that

$$\left.\begin{aligned}\big(\boldsymbol{\nabla\cdot}\,\boldsymbol{\sigma}_h,q\big)_K - \big(\beta\eta_h,q\big)_K + \big\langle\tau(\eta_h-\lambda),q\big\rangle_{\partial K} &= \big(f,q\big)_K,\\ \big(\mathbf{Q}^{-1}\boldsymbol{\sigma}_h,\boldsymbol{v}\big)_K - \big(\eta_h,\boldsymbol{\nabla\cdot}\,\boldsymbol{v}\big)_K + \big\langle\lambda,\boldsymbol{v}\cdot\boldsymbol{n}\big\rangle_{\partial K} &= 0,\end{aligned}\right\} \qquad \forall K\in\mathcal{T}_h, \tag{6a}$$

$$\begin{aligned}\big\langle\left(\boldsymbol{\sigma}_h\cdot\boldsymbol{n}+\tau(\eta_h-\lambda)\right),\mu\big\rangle_{\partial\mathcal{T}_h} &+ i\big\langle cc_g k\alpha\lambda,\mu\big\rangle_{\Gamma_{\mathrm{R}}}\\ &+ i\big\langle cc_g k\lambda,\mu\big\rangle_{\Gamma_{\mathrm{NRB}}} = \big\langle cc_g\left(\boldsymbol{\nabla}\eta_0\cdot\boldsymbol{n} - ik\alpha\eta_0\right),\mu\big\rangle_{\Gamma_{\mathrm{R}}},\end{aligned} \tag{6b}$$

for all $(\boldsymbol{v},q,\mu)\in\boldsymbol{V}_h\times P_h\times M_h$.
It is worth noting that (6a) is a local system in each element K, which does not involve unknowns of neighboring elements. Thus, (6a) can be solved element-by-element to express $\boldsymbol{\sigma}_h$ and η_h as functions of λ. On the other hand, equation (6b) is the one coupling the variables of different elements. Replacing $\boldsymbol{\sigma}_h$ and η_h, solution of (6a) in terms of λ, in (6b) yields a global system on the whole mesh skeleton for the trace variable, $\lambda\in M_h$, which is single valued in each face F of the mesh. Once the global system is solved, $\boldsymbol{\sigma}_h$ and η_h, can be recovered for each element K using (6a).
For a uniform distribution of p, HDG with the particular choice of the numerical flux in (5) attains optimal convergence rates of order $p+1$ in L_2 norm, for the unknown η_h and also for its derivative $\boldsymbol{\sigma}_h$, see [7] for proof.

This property is the key ingredient for a local element by element post-process of the HDG solution providing a superconvergent solution η_h^* with errors of order $p+2$ in L_2 norm. The problem to be solved in each element K to compute the superconvergent approximation η_h^* is

$$-\boldsymbol{\nabla}\cdot(\nabla\eta_h^*) = \boldsymbol{\nabla}\cdot(\mathbf{Q}^{-1}\boldsymbol{\sigma}_h) \quad \text{in } K, \tag{7a}$$

$$-\nabla\eta_h^*\cdot\boldsymbol{n} = \mathbf{Q}^{-1}\boldsymbol{\sigma}_h\cdot\boldsymbol{n} \quad \text{on } \partial K, \tag{7b}$$

with the additional constrain

$$\int_K \eta_h^*\, d\Omega = \int_K \eta_h\, d\Omega, \tag{8}$$

where $\eta_h^* \in \mathcal{P}^{p+1}(K), \forall K \in \mathcal{T}_h$.
The weak form of equations (7a) and (7b) with constrain (8) is

$$\begin{aligned}\left(\nabla\eta_h^*, \nabla q\right)_K &= -\left(\mathbf{Q}^{-1}\boldsymbol{\sigma}_h, \nabla q\right)_K, \quad \forall\omega \in \mathcal{P}^{p+1}(K),\\ \left(\eta_h^*, 1\right)_K &= \left(\eta_h, 1\right)_K,\end{aligned}$$

to be solved in a element-by-element fashion, for instance with Lagrange multipliers.
In case of non-uniform distributions of p_K, for each element K the post-process solution η_h^* belongs to the corresponding increased space, i.e. $\eta^* \in \mathcal{P}^{p_K+1}(K)$. Despite the superconvergence property of the HDG post-process solution is only proved for uniform p distribution, numerical experiments confirm that the element-by-element post-process solution for non-uniform p distributions improves the accuracy of the computation. Thus, for an adaptive computation, the goal is to consider the post-process solution to obtain an error estimator in each element through a low cost element-by-element computation.

3 NUMERICAL EXPERIMENTS

This section is devoted to presenting a preliminary comparison, with uniform p-distribution, between HDG, CG and CDG. The comparison is carried out for different values of p, on the basis of the dimension of the linear system and the total computing time. The goal is to highlight, on one hand, the convenience of using high order elements for a wide range of wavelengths, even for engineering accuracy. On the other hand, similar performance for the HDG and CG methods are shown, when properly choosing the p for a desired error level and wavelength. Both HDG and CG are clearly outperforming the CDG method.
The test problem is the scattering of a plane wave by a cylindrical object of radius=1m, in a square domain of side 5m. An even bottom is considered: the MSE reduces in this case to the Helmholtz equation. An analytical solution to this problem can be found in [16]. Three different values of the incident wave period are tested, $T = 0.2s, 0.4s$ and $0.6s$. The bottom depth is set to 1m, generating a number of waves in the domain varying from 17 to 160. Triangular meshes are used. Figure 1 depicts the convergence curves for $T = 0.2s$ and $0.6s$, for the L_2 error of the approximated solution evaluated in the whole domain (the two upper figures) and on the scattering boundary (the two lower figures). The points on each curve are at fixed number of nodes per wavelength, with values of $k\Delta x = 0.5, 0.75, 1, 1.25$, being Δx the element size h divided by p. The post-processed solution is considered for the HDG method. At the bottom of each curve, the mean slope of the curve is also displayed. It is interesting to note that the slope of the curves is in general higher for a lower period, i.e. where the dispersion error is dominating. In fact, as shown in [17], the dispersion error decreases with slope h^{2p} while the interpolation error decreases with slope h^{p+1}. In general, it is possible to conclude that discontinuous methods are less affected by the dispersion at low p, giving less error for the same computational mesh. This difference becomes smaller increasing the polynomial degree. For high order elements, CDG is attaining the same precision (or less) than CG, but obviously using more DOF. These curves also highlight how increasing the element order it is possible to reduce the number of nodes per wave length for a given precision.
In Figure 3, the number of DOF for a fixed value of the error are depicted. The number of DOF for each error level are estimated from the convergence curves Figure 1. The value is linearly interpolated in log-log scale, when the chosen error level is laying between the limits of the convergence curve, otherwise it is linearly extrapolated using the closest two points. For linear elements, only the HDG curve is drawn for the interpolated error in the whole domain, since extrapolation for CG and CDG is not feasible since the curves are not in the asymptotic range. Increasing p, less degrees of freedom are needed for a given precision level for HDG and CG. CDG is always using more DOF than the other two methods for the same p. Conclusions are the same considering the error in the domain and in the boundary.

From these results, the first comparison is discarding $p = 1$ for any method and CDG for any p. CG and HDG are further compared next in terms of computing time, taking into account matrix set up (assembly), linear system solution and post-processing. The quadrature considered for time computation purpose are not considering the overhead due to curved elements, that are a small percent of the whole element set. Thus, the following quadrature for triangles are used:

Table 1: Quadrature rules for various p.

p	**1**	**2**	**5**	**9**
Order	2	5	10	20
N. Gauss points	3	7	25	85

For the linear system solution, a direct solver is considered. Figure 3 depicts the global computing time for the CG and HDG method. A part from the matrix assembly and the linear system solution time, common to both methods, the time to recover the inner node values is added for CG, while for HDG, the elemental solution reconstruction and the postprocess time is also taken into account. The value is interpolated from the convergence curves, in the same way as for the DOF. High order elements are requiring less computing time than low order ones. High order computations $p = 5$ and $p = 9$ are giving similar performance, the best choice depending on the accuracy level required and the wave length. Lowering the accuracy and the wave length moves the optimum point to higher p. While for low orders HDG is clearly outperforming CG, for high orders the two methods have similar performance.

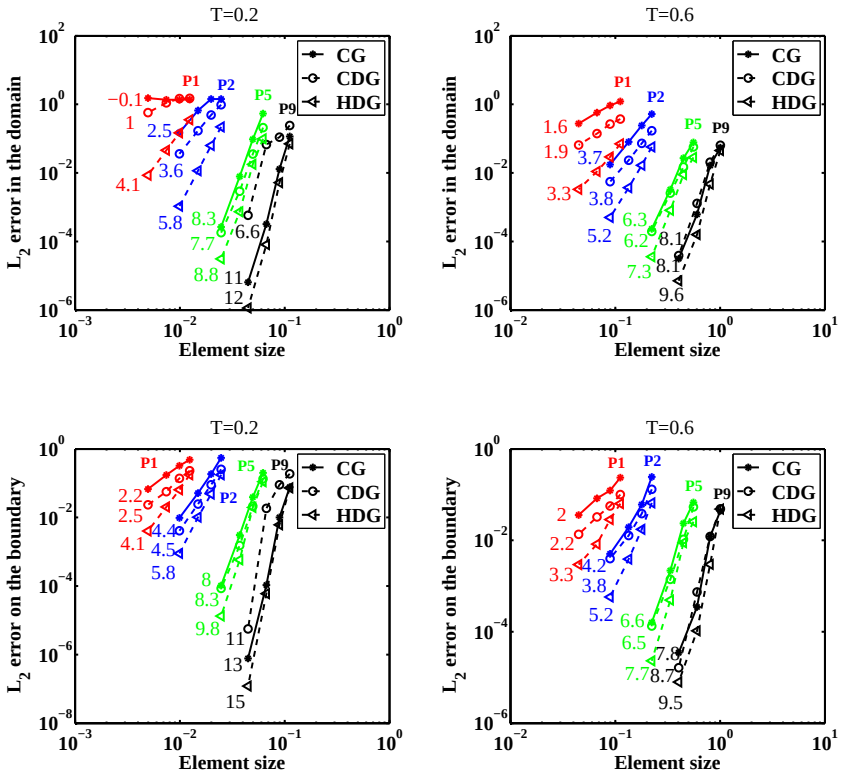

Figure 1: Convergence curves for the three methods: (top) error in the whole domain, (bottom) error in the boundary

4 ERROR ESTIMATION AND *P*-ADAPTIVE ALGORITHM

In this section, the p-adaptive technique is described, focusing on the problem of wave agitation in harbors. The typical quantity of interest for this problem is the wave height, $H \in \mathbb{R}^+$, in each point of the interior of the harbor,

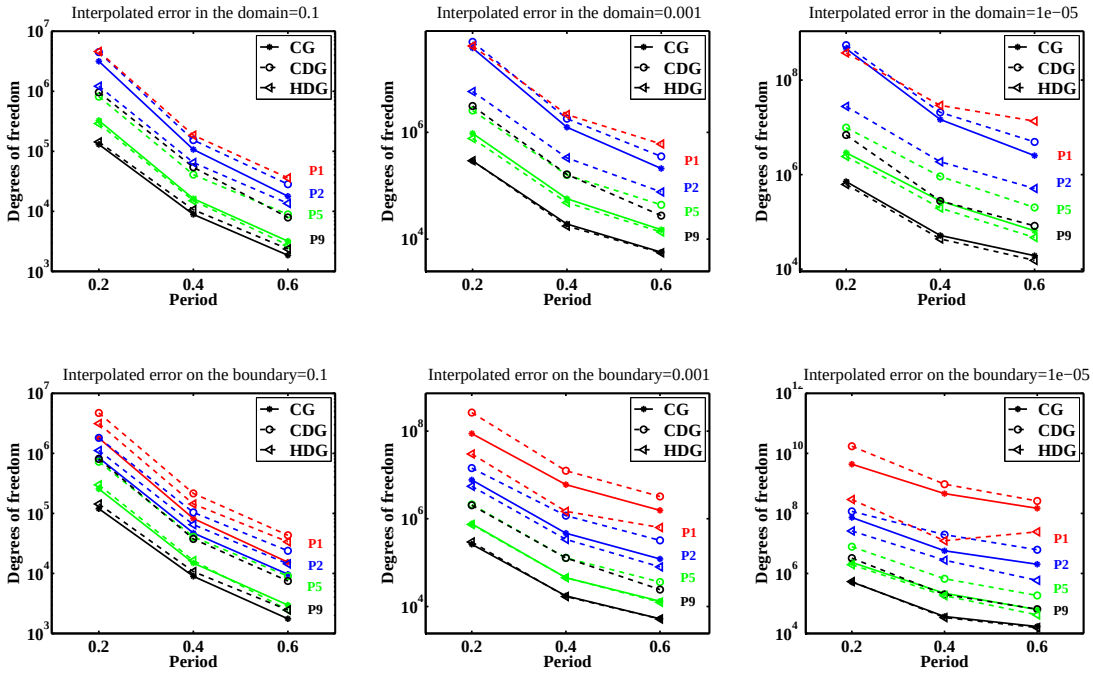

Figure 2: Number of DOF for an accuracy of (left) 1e-1, (center) 1e-3, (right) 1e-5, (top) in the domain, (bottom) on the boundary.

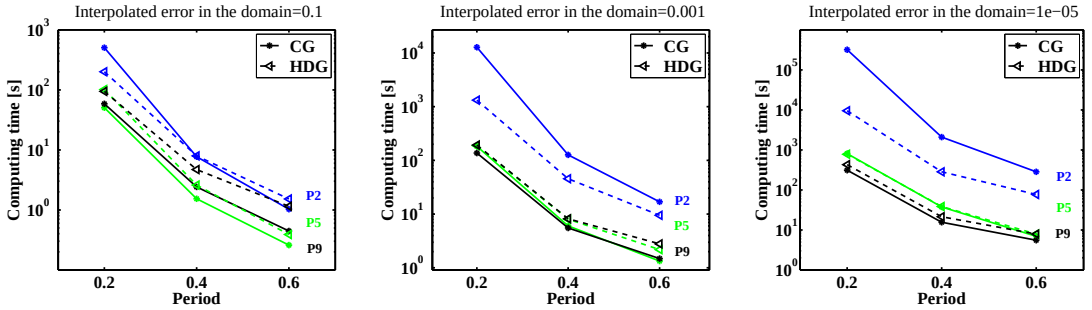

Figure 3: Computing time for an accuracy of (a) 1e-2, (b) 1e-3, (c) 1e-5 in the whole domain.

which can be expressed as a function of the incident wave height H_0 and the solution η, from the *wave amplification factor* formula

$$\frac{H}{H_0} = |\eta + \eta_0|.$$

Hence, calling A_{int} the area of the zone of interest, the error in the quantity of interest is

$$E = \sqrt{\int_{\Omega_{int}} \frac{(H^{ex} - H)^2 \, d\Omega}{A_{int}}}, \tag{9}$$

i.e., the L_2 norm computed on the zone of interest, of the difference between the approximation of the wave height and its exact value H^{ex}. The goal of the adaptive procedure is to reduce the error defined in (9) until a tolerance ε, modifying iteratively the polynomial degree in each element. An *a posteriori* error estimator is needed to measure the elemental contribution to the global error in the zone of interest, and drive the p-adaptive refinement. There are several methods to derive an *a posteriori* error estimator, see for example [18] for an exhaustive survey. Error indicators are usually based on the approximated solution and thus cheap to evaluate, see [19] for a discussion,

and are usually preferred in transient or non-linear problems where repeated error maps are required. On the other hand, *a posteriori* residual-type or recovery-based error estimators provide accurate error estimates or bounds of quantities of interest, but with an important computational cost. In HDG, the superconvergent post-process appears as the natural choice for the computation of an enhanced solution to estimate the error. The error in each element is estimated as

$$E_K = \sqrt{\int_K \frac{(H^* - H)^2 \, d\Omega}{A_K}}, \tag{10}$$

where H^* is the wave height computed with the post-process solution and A_K is the element area, see also [20]. The post-process solution in the case of uniform p_K provides an asymptotically exact estimator, and in case of non-uniform p_K distribution, numerical examples confirm the reliability of this estimator.

The procedure considered for the definition of the adaptive process is described next. In a generic iteration of the adaptive process, the solution is computed with a p_K-map of interpolation degrees. A map of elemental error is then estimated with equation (10), which allows to evaluate a new p_K-map, to improve the solution. The update of the p_K-map is done in two steps: in the first step, the p_K variation in each element is computed as

$$\Delta p_K = \lceil \log_b(\frac{E_K}{\epsilon_K}) \rceil, \tag{11}$$

where ϵ_K is a tolerance and the logarithmic base b is a user defined value, see [21]. The tolerance ϵ_K represents the desired level of error in the element K, and different values of ϵ_K for different elements can be used, to refine more in the zone of interest of the domain. Parameter b controls the behavior of the adaptive procedure: for a fixed elemental error E_K, increasing b has the effect to decrease the variation Δp_K corresponding to E_K. Thus, small values of b yield fast refinement with fast convergence to an accurate enough approximation, but too refined and computationally expensive in some cases; on the contrary, large values of b yield slow refinement, and the necessity for repeated computation to achieve the desired level of error in some cases.

In addition, the polynomial degree is modified in each element to comply with the bounds $p_{min} \leq p_K \leq p_{max}$, being p_{min} and p_{max} respectively the minimum and maximum value of the polynomial degree allowed in the mesh: if the computed p_K is out of range, p_{max} or p_{min} is used instead. The value of p_{min} is chosen to guarantee a minimum number of nodes per wavelength in all the elements. The choice of using a value $p_{max} < \infty$ to limit the maximum polynomial degree in the mesh mainly depends on implementation issues, such as available quadrature rules, and user preferences. In practice, for a harbor agitation study, the incident wave hardly enters the zone of interest and no resonance are expected. Thus,computational experiments show that, for engineering accuracy, a good choice is a constant discretization with elements size h $\approx L$, where L is the wavelength, achieving convergence with a maximum $p_K \approx 10$. In addition, to exploit the characteristic of HDG to reduce the coupled DOF for high-order elements, an efficient option is to use large elements and $p_{min} > 2$.

It is worth nothing that the p_K-map resulting from this first step can present neighboring elements with large difference in polynomial degree. To prevent too sharp spatial variation of p_K, in the second step of the refinement process a smoothing of the p_K-map can be performed, to guarantee that the difference in polynomial order between two neighboring elements is not greater than a given value δ. The smoothing process consists in an iterative process in which, for $p = \max\{p_K\}, \max\{p_K\} - 1, \ldots, p_{min}$, the degree of all the elements K sharing a face with a p-th order element is set to $\max\{p - \delta, p_K, p_{min}\}$. In the numerical tests of this paper, the maximum difference δ in polynomial degree between two neighboring elements is fixed to 1.

The computation is typically carried out in the first stage on a uniform mesh with $p_K = p_{min}$ and the mesh adaptation process goes on until a desired precision ε is achieved in the zone of interest. For $p_{max} < \infty$, the required level of precision may be unreachable for a given mesh. In this case, the process stops if in two successive p_K-maps the percentage of elements changing their p is lower than a given tolerance.

5 WAVE PROPAGATION IN HARBORS

In this example the wave propagation in the Mataró harbor, whose picture is shown in Figure 4(a), is simulated. The docking area is considered as the zone of interest of the domain. Figure 4(b) depicts the computational domain, highlighting the PML and the zone of interest. The physical boundaries, also shown in Figure 4(b), are modeled as absorbing boundaries with α=0.02 for dikes, α=0.4 for breakwaters and α=0.7 for beaches. The incident potential direction is 10° from the x-axis, which should induce non-negligible agitation in the interior. The wave period is 5s, corresponding to short waves with a maximum value of the wavelength of about 40m, in the PML region, and a minimum value of 25m, in the interior of the harbor and close to the beach. The bottom depth has been set using real

data of bathymetric campaigns (see *www.portmataro.com*) and then smoothed to comply the condition of constant bottom depth in the PML area, which is crucial for the correct absorption of the PML.
The high-order meshing software ez4u (see *www.lacan.upc.edu/ez4u.htm*) is used to generate an unstructured triangular mesh of uniform element size h=40m in the whole domain, except the interior of the harbor where the mesh size varies locally to capture the geometrical features of the docking area. The wave amplification factor in the domain is displayed in Figure 5(a): it is worth nothing the increase of the wave height due to the bathymetry approaching the beach outside the harbor.
In Figure 5(b), the p convergence of the CG method and the HDG method is compared with a p_K-variable HDG convergence curve. For the p_K-variable HDG method, starting from a uniform mesh $p = 4$, in each iteration an element by element error estimate E_K is computed as (10) and then p_K is increased of 1 in those elements where the error is greater than 10% of the max estimated error E_K^{max} in the domain. That is, in each iteration a variable p_K-map is considered with $4 \leq p_K \leq p_i$, with $p_i = 4, 5, .., 11$. The exact error of the post-processed solution is plotted for each iteration as a function of the number of DOF of the p_K-variable computation. These curves illustrate the convenience of the p-adaptive technique, which allows to reduce considerably the number of DOF of the computation, providing better performance not only than p-uniform HDG but also CG. This test also shows the reliability of the error estimator in the task of driving an adaptive process.
The adaptive procedure described in Section 4 is used to compute the wave amplification factor in the Mataró harbor. Three values of desired precision in the zone of interest ε are considered: 5e-2, 1e-2 and 5e-3. The elemental tolerance ϵ_K is set to the half of ε if the element is in the zone of interest, and the double of ε if the element is outside the zone of interest. No maximum degree is fixed, i.e. $p_{max} = \infty$, and the minimum p allowed in the mesh is set to 4, guaranteeing a minimum of 4 nodes per wavelength in the PML region. The coefficient b controlling the velocity of the adaptive process in (11) is set to 3. The adaptive process converges in 1 iterations in the three cases. Figure 6(a) depicts the p_K distribution obtained for the case $\varepsilon =$ 1e-2. As expected, the method drives the mesh refinement to reduce the error in the area of decreasing bathymetry and wave interactions. Although the wave amplification factor is very small in the interior of the harbor, the polynomial degree increases in the docking area due to the smaller tolerance set in the zone of interest. A comparison of the number of DOF of the computation for the adaptive HDG with non adaptive HDG and CG computations is shown in Figure 6(b). The proposed adaptive HDG requires less DOF at equal level of error compared to HDG and also CG.

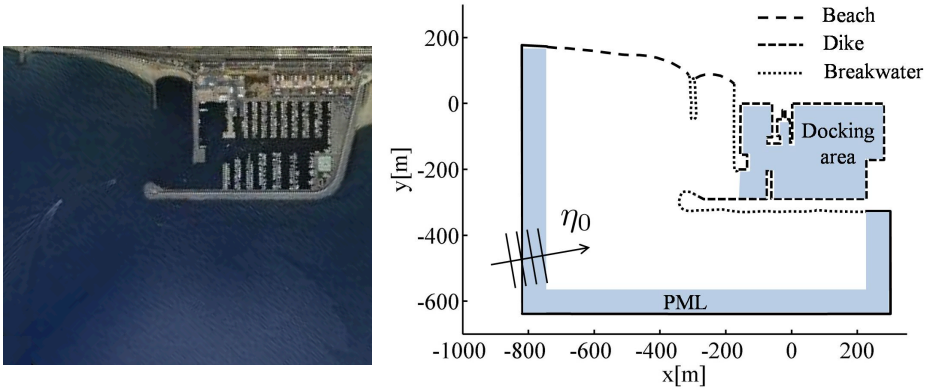

(a) Picture of the Mataró harbor

(b) Computational domain, boundary conditions and incident potential

Figure 4: Problem statement for the Mataró harbor. Values of α: dikes-0.02; breakwaters-0.4; beaches-0.7

6 CONCLUSIONS

The HDG method is applied to the problem of stationary non-homogeneous wave propagation in an open domain. The hybridization technique allows to reduce drastically the number of DOF of the computation, solving a system of equations involving unknowns only on the sides of the mesh, and opens the path to a post-process of the solution resulting in a superconvergent solution.

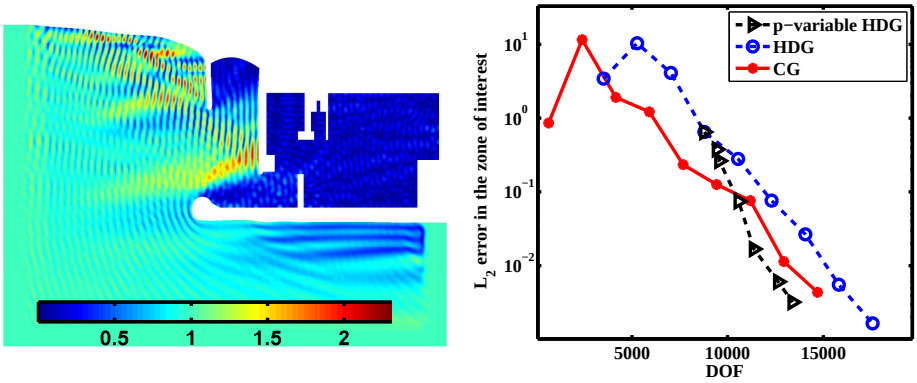

Figure 5: Wave amplification factor in the Mataró harbor (left) and $p = 1 \cdots 9$ convergence for the CG and HDG methods compared with a p-variable HDG computation (right).

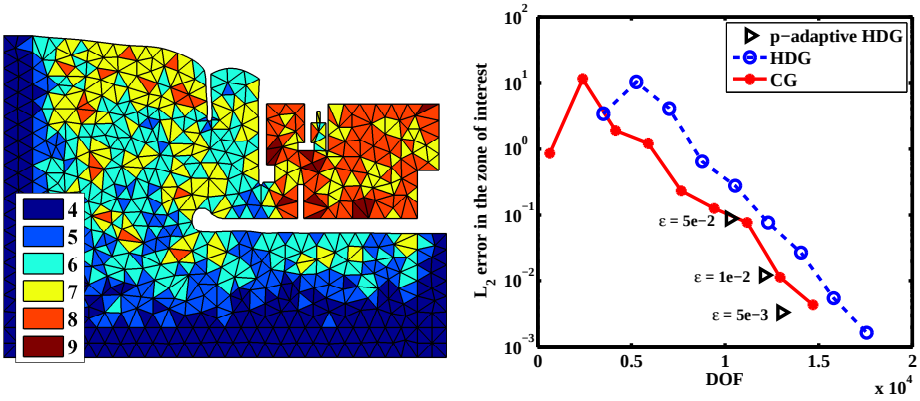

Figure 6: p-map for $\epsilon = 10^{-2}$ (left) and the number of DOF of the computations for the p-adaptive HDG method proposed in Section 4 (right).

A performance comparison between HDG, CG and CDG, based on the number of DOF of the linear system and global computing time, is presented for a simple geometry. Results highlight the superiority of high-order elements, and similar performance for CG and HDG, clearly surpassing CDG, when adopting the best choice of p for a selected error level and a given wave length.

The superconvergent post-process of the HDG method is used to construct a simple error estimator based on the L_2 difference between the wave height computed with the solution and the post-processed solution. The error estimator is used to drive an iterative procedure of mesh adaptation aimed at reaching a desired level of error in the zone of interest of the domain. A simple strategy of adaptivity orientation is also used in order to concentrate the refinement process in the zone of interest.

A real case of wave propagation in a harbor is presented. Fast convergence to the desired level of precision is proved. A comparison based on the number of DOF of the linear system is carried out between the proposed adaptive HDG method and CG. The adaptive HDG method exhibits the best computational efficiency in term of DOF for the problem studied.

REFERENCES

[1] S. J. Sherwin, R. M. Kirby, J. Peir, R. L. Taylor, and O. C. Zienkiewicz. On 2D elliptic discontinuous Galerkin methods. *International Journal for Numerical Methods in Engineering*, 65(5):752–784, 2006.

[2] J. Peraire and P. O. Persson. The compact discontinuous Galerkin (CDG) method for elliptic problems. *SIAM J. Sci. Comput.*, 30(4):1806–1824, 2008.

[3] G. Gabard, P. Gamallo, and T. Huttunen. A comparison of wave-based discontinuous Galerkin, ultra-weak and least-square methods for wave problems. *International Journal for Numerical Methods in Engineering*, 85(3):380–402, 2011.

[4] X. Feng and H. Wu. Discontinuous Galerkin methods for the Helmholtz equation with large wave number. *SIAM J. Numer. Anal.*, 47:2872–2896, August 2009.

[5] G. Benitez Alvarez, A. F. Dourado Loula, E. Gomes Dutra do Carmo, and F. Alves Rochinha. A discontinuous finite element formulation for Helmholtz equation. *Computer Methods in Applied Mechanics and Engineering*, 195(33-36):4018 – 4035, 2006.

[6] B. Cockburn and J. Gopalakrishnan. A characterization of hybridized mixed methods for second order elliptic problems. *SIAM Journal on Numerical Analysis*, 42(1):pp. 283–301, 2005.

[7] B. Cockburn, B. Dong, and J. Guzmán. A superconvergent LDG-hybridizable Galerkin method for second-order elliptic problems. *Mathematics of Computation*, 77(264):1887–1916, 2008.

[8] N.C. Nguyen, J. Peraire, and B. Cockburn. A hybridizable discontinuous Galerkin method for Stokes flow. *Computer Methods in Applied Mechanics and Engineering*, 199(9-12):582–597, 2010.

[9] R. Kirby, S. Sherwin, and B. Cockburn. To CG or to HDG: A comparative study. *Journal of Scientific Computing*, pages 1–30, 2011.

[10] M.S. Shephard, S. Dey, and J.E. Flaherty. A straightforward structure to construct shape functions for variable p-order meshes. *Computer Methods in Applied Mechanics and Engineering*, 147(3-4):209 – 233, 1997.

[11] P. R. B. Devloo, C. M. A. Ayala Bravo, and E. C. Rylo. Systematic and generic construction of shape functions for p-adaptive meshes of multidimensional finite elements. *Computer Methods in Applied Mechanics and Engineering*, 198(21-26):1716 – 1725, 2009.

[12] K. Kim, D. Yi, and S. Lee. Mortar method for nonconforming finite elements. *Applied Mathematics and Computation*, 167(1):650 – 669, 2005.

[13] J. C. W. Berkhoff. Computation of combined refraction-diffraction. In *Proceedings of the 13th Coastal Engineering Conference*, volume 1, pages 471–490, ASCE: Vancouver, Canada, 1972.

[14] N. Booij. A note on the accuracy of the mild-slope equation. *Coastal Engineering*, 7(3):191 – 203, 1983.

[15] Jean-Pierre Berenger. A perfectly matched layer for the absorption of electromagnetic waves. *J. Comput. Phys.*, 114:185–200, October 1994.

[16] R. A. Fuchs R. C. MacCamy. Wave forces on piles: a diffraction theorys. Technical report, US Army Corps of Engineering, Beach Erosion Board, Washington, DC, 1954.

[17] F. Ihlenburg and I. Babuka. Dispersion analysis and error estimation of Galerkin finite element methods for the Helmholtz equation. *International Journal for Numerical Methods in Engineering*, 38(22):3745–3774, 1995.

[18] T. Grätsch and K.-J. Bathe. A posteriori error estimation techniques in practical finite element analysis. *Comput. Struct.*, 83:235–265, January 2005.

[19] A. Huerta, A. Rodrguez-Ferran, P. Dez, and J. Sarrate. Adaptive finite element strategies based on error assessment. *International Journal for Numerical Methods in Engineering*, 46(10):1803–1818, 1999.

[20] C. Eskilsson. An hp-adaptive discontinuous Galerkin method for shallow water flows. *International Journal for Numerical Methods in Fluids*, pages n/a–n/a, 2010.

[21] J.-F. Remacle, J. E. Flaherty, and M. S. Shephard. An adaptive discontinuous Galerkin technique with an orthogonal basis applied to compressible flow problems. *SIAM Review*, 45(1):53–72, 2003.